Synchronous Physical-Layer Network Coding: A Feasibility Study

Yang Huang, *Student Member, IEEE*, Shiqiang Wang, *Student Member, IEEE*, Qingyang Song, *Member, IEEE*, Lei Guo, *Member, IEEE*, and Abbas Jamalipour, *Fellow, IEEE*

***Abstract*—Recently, physical-layer network coding (PNC) attracts much attention due to its ability to improve throughput in relay-aided communications. However, the implementation of PNC is still a work in progress, and synchronization is a significant and difficult issue. This paper investigates the feasibility of synchronous PNC with M-ary quadrature amplitude modulation (M-QAM). We first propose a synchronization scheme for PNC. Then, we analyze the synchronization errors and overhead of potential synchronization techniques, which includes phase-locked loop (PLL) and maximum likelihood estimation (MLE) based synchronization schemes. Their effects on the average symbol error rate and the goodput are subsequently discussed. Based on the analysis, we perform numerical evaluations and reveal that synchronous PNC can outperform conventional network coding (CNC) even when taking synchronization errors and overhead into account. The theoretical throughput gain of PNC over CNC can be approached when using the MLE based synchronization method with optimized training sequence length. The results in this paper provide some insights and benchmarks for the implementation of synchronous PNC.**

***Index Terms*—Communication; denoise-and-forward (DNF); physical-layer network coding (PNC); synchronization; two-way relay networks.**

I. Introduction

Relay-aided communications are widely adopted when direct communications among end nodes cannot be performed. Physical-layer network coding (PNC) [2] is considered as a promising technology to improve the throughput performance of relay networks. It employs the natural network coding ability introduced by the superposition of electromagnetic waves. Between the two methods of PNC, i.e. amplify-and-forward [3] and denoise-and-forward (DNF), the DNF method shows more performance advantages because it avoids noise amplification [4]. Hence, DNF has attracted much interest in recent research, and this paper considers the DNF scheme. We use DNF and PNC interchangeably in subsequent discussions.

Research regarding PNC has been carried out focusing on two aspects: phase-asynchronous PNC [5]–[7] and phase-synchronous PNC [8]–[12]. The basic idea of asynchronous PNC is to map the superposed signal with arbitrary phase differences to encoded symbols. However, these schemes require knowledge of the instantaneous phases of the signals superposing at the relay, and imperfect channel information may also degrade the performance of asynchronous PNC [13]. Hence, tracking phase variations[1] during data packet transmission is necessary (although synchronization is not needed), which can be difficult especially for the superposed signal. The complexity of obtaining symbol mapping under various phase differences can also be high, in particular with high-level modulations [5]. Compared with asynchronous PNC, synchronous PNC allows more efficient constellation design [8] and can make use of capacity-approaching channel codes [11]. The capacity region of the Gaussian two-way relay channel can also be reached with synchronous PNC [12]. Further, [14] shows that compared with other schemes, phase synchronization can maximize the minimum distance between adjacent points in the constellation for superposed signals, provided that the signals are with the same modulation and amplitude at the relay. Therefore, we focus on the phase-synchronous PNC in this paper.

Synchronization is a significant issue for synchronous PNC, which, however, has not been adequately studied. Existing works [8]–[12] generally assume that superposing signals arrive in-phase at the relay. However, these works have not addressed how to achieve such a synchronization, to the best of our knowledge. Although [15] investigated the impact of imperfect synchronization for binary phase-shift keying (BPSK) modulated PNC, it did not explicitly introduce a synchronization scheme and also did not investigate the interaction between synchronization and data transmission. In the literature, some phase synchronization schemes for distributed beamforming have been studied [16]–[19]. Although both PNC and distributed beamforming make use of signal superposition, the goal of PNC is to increase network throughput, while distributed beamforming is for increasing the signal strength at the receiver. Meanwhile, the end nodes cannot communicate with each other when using PNC (otherwise relaying is unnecessary); while in beamforming, the

Some preliminary ideas of this paper have been presented in IEEE GLOBECOM 2012 [1].

This work was supported in part by the National Natural Science Foundation of China (61172051), the Fok Ying Tung Education Foundation (121065), the Fundamental Research Funds for the Central Universities (N110204001, N110804003, N120804002, N120404001), the Program for New Century Excellent Talents in University (NCET-12-0102), and the Specialized Research Fund for the Doctoral Program of Higher Education (20110042110023, 20110042120035, 20120042120049).

Y. Huang, Q. Song (corresponding author) and L. Guo are with School of Information Science and Engineering, Northeastern University, Shenyang 110819, P. R. China. Email: yang.huang@ieee.org, {songqingyang, guolei}@ise.neu.edu.cn.

S. Wang is with Department of Electrical and Electronic Engineering, Imperial College London, SW7 2AZ, United Kingdom. Email: shiqiang.wang11@imperial.ac.uk.

A. Jamalipour is with School of Electrical and Information Engineering, University of Sydney, NSW, 2006, Australia. Email: a.jamalipour@ieee.org.

[1] Note that frequency errors accumulate over time and may cause the phase difference between the two superposed signals change continuously.

Fig. 1. PNC over a two-way relay network.

end nodes (sensors) may communicate with each other. The difference between these two techniques can make synchronization schemes for beamforming infeasible for PNC. The limited feedback-based synchronization for beamforming such as [16] may cause large synchronization overhead due to the iterative process, which violates the intention of PNC, since the overhead can reduce the goodput (i.e. effective throughput). Open-loop schemes as in [17]–[19] are also inapplicable for PNC, because they require the end nodes to communicate with each other. Moreover, synchronization schemes for PNC do not need to consider large-sized networks, because only two nodes (rather than multiple nodes as in beamforming) are generally involved in the PNC process [20]. To consider the requirements of PNC, in this paper, we propose a phase synchronization scheme for PNC.

Based on the proposed synchronization scheme, we discuss synchronization errors arising during the phase synchronization process and their impacts on the symbol error rate (SER) and network goodput in this paper. In terms of SER analysis for PNC, [21] derived the SER for PNC with perfect synchronization and unequal power of the superposing signals. Assuming the knowledge of channel gains, the SER for PNC with decoding methods that do not require phase synchronization are discussed in [22] and [23], which respectively focus on minimum distance estimation and maximum a posteriori based decoding methods. The above existing works did not consider phase variations that may result from synchronization errors. In our preliminary work [24], we focused on SER of PNC with deterministic phase deviations. In this paper, we focus on random phase deviations due to random synchronization errors. We derive analytical expressions of the average SER for PNC with M-ary quadrature amplitude modulation (M-QAM), and subsequently study the impact of synchronization errors and overhead to the network goodput.

We consider a two-way relay network as shown in Fig. 1. The main contribution of this paper is outlined as follows:

1) We propose a phase synchronization scheme for PNC, which takes into account the characteristics and requirements of PNC as aforementioned. The synchronization errors of the proposed synchronization scheme are then analyzed by considering potential frequency and phase estimation techniques, namely, analog phase-locked loop (PLL), which is a conventional approach, and maximum likelihood estimation (MLE), which is a more sophisticated but accurate approach.
2) We derive analytical expressions and their approximate solutions of the average SER for M-QAM modulated PNC under the presence of synchronization errors. Random synchronization errors which accumulate and vary over time are considered. The analytical results are then verified via simulations.
3) We consider the joint operation of synchronization and data transmission, and study the goodput of the two-way relay network. The feasibility of phase-synchronous PNC is shown by numerical results.

In summary, we present a phase synchronization scheme for PNC and study the interactions between the synchronization overhead, accuracy, SER, and network goodput, under estimation methods with PLL and MLE. Such a study enables us to understand whether phase-synchronous PNC is feasible or beneficial when incorporating with the synchronization procedure that uses common estimation methods. The analytical results also allow us to optimize the length of the training sequence that is used for synchronization (as will be discussed in Section V-B). Meanwhile, the framework that we use for analysis can be applied when other estimation methods and/or noise sources are considered.

The remainder of this paper is organized as follows. Section II illustrates the system model of this paper. Section III introduces the phase-level synchronization scheme and analyzes errors with different estimation methods. In Section IV, the average SER under the impact of synchronization errors is discussed. The goodput of synchronous PNC is analyzed in Section V. Conclusions are drawn in Section VI.

II. System Model

We consider a typical bidirectional relay network with flat fading channels, and the relay node R performs DNF relaying, as shown in Fig. 2. The DNF process includes multiple access (MA) phase and broadcast (BC) phase. Without loss of generality, we focus on square M-QAM modulated PNC in this paper, and end nodes A and B simultaneously transmit square M-QAM modulated data to the relay in the MA phase. The case of some common non-square M-QAM modulations (such as 32-QAM) can be treated similarly as square M-QAM, as discussed in [10]. The signal Y_R received by R is given by

$$Y_R = S_A + S_B + Z_{n,R}\,, \tag{1}$$

where S_A and S_B denote M-QAM signals from A and B respectively, and $Z_{n,R}$ is the additive white Gaussian noise (AWGN) at R. In this paper, we consider the case where the average powers of S_A and S_B are equal.

The minimum distance estimation is employed at the relay R to map the superposed signal Y_R to a network-coded symbol. In this paper, PNC is performed with phase-level synchronization to maximize Euclidean distances, i.e. each constellation point (ideally) appears in the center of the corresponding decision region.

Because a M-QAM signal can be viewed as a complex $\sqrt{M}$-ary pulse amplitude modulation ($\sqrt{M}$-PAM) signal, its in-phase component $I_R(m_\Sigma)$ and quadrature component $Q_R(n_\Sigma)$ can be extracted from the superposed constellation point S_{m_Σ,n_Σ}, i.e. $S_{m_\Sigma,n_\Sigma} = I_R(m_\Sigma) + jQ_R(n_\Sigma)$. The scalar values of these components are given by $I_R(m_\Sigma) = 2(m_\Sigma - \sqrt{M})d_0$ and $Q_R(n_\Sigma) = 2(n_\Sigma - \sqrt{M})d_0$, where $m_\Sigma, n_\Sigma \in \{1, 2, \cdots, 2\sqrt{M} - 1\}$ denote indices of constellation points for the superposed signal, and d_0 represents the Euclidean distance between two adjacent points in the

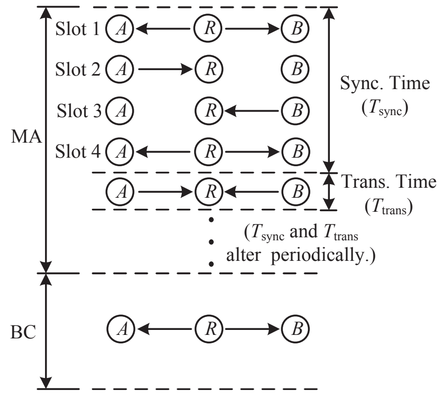

Fig. 2. Network topology and timing diagram. Synchronization (sync.) and transmission (trans.) alternate over the multiple access (MA) phase, and they are performed periodically.

constellation diagram for $\sqrt{M}$-PAM. The minimum distance estimation for $\hat{S}_{m_\Sigma,n_\Sigma}$ is given as

$$(\hat{m}_\Sigma, \hat{n}_\Sigma) = \arg\min_{m_\Sigma,n_\Sigma} |Y_R - (I_R(m_\Sigma) + jQ_R(n_\Sigma))|, \quad (2)$$

$$\hat{S}_{m_\Sigma,n_\Sigma} = I_R(\hat{m}_\Sigma) + jQ_R(\hat{n}_\Sigma), \quad (3)$$

where $|\cdot|$ stands for the modulus (absolute value).

The estimated $\hat{S}_{m_\Sigma,n_\Sigma}$ will be mapped into a network-coded symbol with the approach proposed in [10].

III. Phase Synchronization

This section firstly introduces a round-trip estimation based carrier synchronization scheme for PNC. Afterwards, we analyze phase synchronization errors when performing phase and frequency estimation using PLL and MLE, respectively.

A. Synchronization Process

As depicted in Fig. 2, the synchronization phase (whose length is denoted as the synchronization time T_{sync}) is divided into four timeslots.

In timeslot 1, the relay R broadcasts a beacon $b_0(t) = a_0 \cos(\omega_c t + \phi_0)$, where a_0 represents the amplitude of this sinusoidal signal, ω_c denotes the reference angular frequency, and ϕ_0 is the initial phase at $t = 0$. The received beacon $b_{R,A}(t)$ at end node A (because the case for node B is similar, we only focus on node A in the subsequent discussions) is given by

$$b_{R,A}(t) = a_{R,A} \cos(\omega_c t + \phi_{R,A}) + Z_{n,A}\,, \quad (4)$$

where $a_{R,A}$ and $\phi_{R,A}$ respectively denote the amplitude and phase of the received signal, and $Z_{n,A}$ denotes the AWGN at node A. Upon receiving $b_{R,A}(t)$, node A estimates the value of ω_c as $\hat{\omega}_c$. Then, node A adjusts its local oscillator to generate a sinusoidal signal with frequency $\hat{\omega}_c$. The same estimation and recovering process is performed at node B. By this means, we achieve frequency synchronization between nodes A and B; and the remaining timeslots are for phase synchronization.

In timeslot 2, the recovered beacon at A is bounced back to the relay R. The signal that is received by node R is given by

$$b_{A,R}(t) = a_{A,R} \cos(\hat{\omega}_c t + \phi_{A,R}) + Z_{n,R}\,, \quad (5)$$

where $a_{A,R}$, $\phi_{A,R}$, and $Z_{n,R}$ respectively denote the amplitude, phase, and AWGN at node R. The relay R estimates the phase $\phi_{A,R}$ of the received signal, and the estimation result is denoted by $\hat{\phi}_{A,R}$. The process is similar for node B in timeslot 3.

In timeslot 4, the relay R transmits the difference between the estimated phase $\hat{\phi}_{A,R}$ and a reference phase ϕ_{ref} back to the end node A for compensation. The reference phase ϕ_{ref} can be set to an arbitrary value (for instance ϕ_0), because we only require that the signals arrive in-phase at R. The operation for node B is same as the above. After compensation, the signals from nodes A and B arrive in-phase (both aligned to ϕ_{ref}) at the relay R.

In the transmission phase (whose length is denoted as the transmitting time T_{trans}) that follows, the recovered signal is used as the carrier signal. Unfortunately, the frequency estimation error causes the phase error increase with time. Therefore, as shown in Fig. 2, synchronization needs to be performed periodically over the MA phase. The synchronization period also needs to be within the duration that channel state remains almost unchanged.

B. Synchronization Errors

Estimation errors occur during synchronization, because received beacons are interfered with AWGNs as in (4) and (5). Thus, $\omega_c = \Delta\omega_c + \hat{\omega}_c$ and $\phi_{A,R} = \Delta\phi_{A,R} + \hat{\phi}_{A,R}$, where $\Delta\omega_c$ and $\Delta\phi_{A,R}$ represent corresponding error terms. The error $\Delta\omega_c$ occurs at the end node, and the error $\Delta\phi_{A,R}$ occurs at the relay, as discussed in Section III-A. The frequency error $\Delta\omega_c$ also results in a linearly increasing phase error during data transmission, which makes the phases of the two signals misalign at the relay and hence increases the average SER.

The errors vary with different estimation methods. In the subsequent discussion, we focus on error analysis for estimation with PLL and MLE, respectively. Note that, although frequency and phase estimation are respectively (not concurrently) performed at the end nodes and the relay, we analyze both frequency and phase errors in the subsequent discussion. The reason is that PLL and MLE can estimate both frequency and phase. Meanwhile, in a general network, each node may have both roles of end node and relay [25]. The specific role depends on the traffic pattern of the network. In such cases, the estimation module can be reused for estimating the frequency and phase. When necessary, we use subscripts "PLL" and "MLE" to represent variables in the corresponding cases.

C. Synchronization Error with PLL Based Estimation

In this subsection, we consider the scenario that a PLL is adopted in the nodes to track the frequency and phase. We derive analytical expressions of the variances of estimation errors through the transfer function of a linearized PLL model. As depicted in Fig. 3, the PLL model consists of a phase detector (PD), a loop filter, and a voltage-controlled oscillator (VCO). The phase of the input (in the S-domain) is denoted by $\phi_{\text{in}}(s)$ and the phase of the VCO output is denoted by $\phi_{\text{out}}(s)$; K_d and K_0 respectively denote the phase-detector gain and the VCO gain; $H_{\text{LF}}(s)$ is the transfer function of the loop filter. In

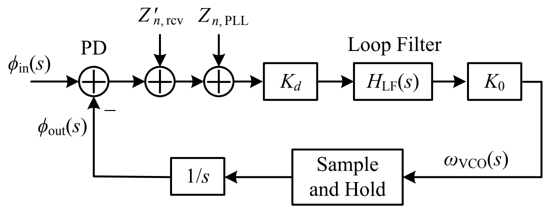

Fig. 3. Linearized PLL model.

timeslot 1, the PLL works in the closed-loop mode, to track the phase and frequency of the reference carrier sent by the relay R. In the remaining timeslots of the synchronization process and also during data transmission, the oscillating frequency $\omega_{\text{VCO}}(s)$ of the VCO is captured by a sample and hold circuit, and the PLL operates in the open-loop mode without further tracking the input signal. The output of the VCO is then used to modulate the data symbols for transmission. Note that the phase difference for compensation can be obtained with an additional phase detector with ϕ_{out} and ϕ_{ref} as the input; phase compensation (as discussed in Section III-A) can be performed on the baseband, i.e. by rotating the signal constellation.

Considering an input such as (4), as discussed in [26], the additive noise term $Z_{n,\text{rcv}}$ at the receiver can be equivalent to $Z'_{n,\text{rcv}}$ as shown in Fig. 3. The power spectral density (PSD) of $Z'_{n,\text{rcv}}$ is $2N_0/a_{\text{rcv}}^2 = N_0 T_s/E_s$, where N_0 denotes the PSD of $Z_{n,A}$, a_{rcv} stands for the received signal amplitude at the receiver, T_s denotes the symbol duration, and E_s denotes the energy per symbol. Meanwhile, $Z'_{n,\text{rcv}}$ is a narrow band noise signal with bandwidth ω_B, because the received signal is processed by a bandpass filter at the receiver. For an ideal receiver that maximizes the bandwidth efficiency, we have $\omega_B = 2\pi/(2T_s)$ for one dimensional signal. The additional noise from the components inside the PLL is denoted by $Z_{n,\text{PLL}}$, which can be conservatively regarded as AWGN with PSD N_p [17].

The value of ω_{VCO} that is captured by the sample and hold component corresponds to the estimated carrier frequency $\hat{\omega}_{c,\text{PLL}}$. Hence, to investigate the error $\Delta\omega_{c,\text{PLL}}$ of frequency estimation, we need to study the noise component at ω_{VCO}. We note that the noise components $Z'_{n,\text{rcv}}$ and $Z_{n,\text{PLL}}$ can also be regarded as the input of the PLL, as shown in Fig. 3. Therefore, the transfer function for noise signal can be evaluated by

$$H(s) = \frac{\omega_{\text{VCO}}(s)}{\phi_{\text{in}}(s)} = \frac{sK_d K_0 H_{\text{LF}}(s)}{s + K_d K_0 H_{\text{LF}}(s)} \,. \tag{6}$$

Considering the respective PSD and bandwidth of $Z'_{n,\text{rcv}}$ and $Z_{n,\text{PLL}}$, we can obtain the variance of the frequency error $\Delta\omega_{c,\text{PLL}}$:

$$\begin{aligned} \sigma^2_{\omega_{c,\text{PLL}}} = {} & \frac{2N_0}{a_{\text{rcv}}^2} \cdot \frac{1}{2\pi} \int_0^{\omega_B} |H(j\omega)|^2 \, d\omega \\ & + N_p \cdot \frac{1}{2\pi} \int_0^{\infty} |H(j\omega)|^2 \, d\omega \,, \end{aligned} \tag{7}$$

where $H(j\omega)$ denotes the system frequency response. Because $Z'_{n,\text{rcv}}$ and $Z_{n,\text{PLL}}$ are Gaussian noises, $\Delta\omega_{c,\text{PLL}}$ conforms to a zero-mean Gaussian distribution given by $\mathcal{N}(0, \sigma^2_{c,\text{PLL}})$.

In the case of a second-order PLL with lag filter (which is frequently used in a wireless repeater [26], for instance), $H(s)$ can be rewritten as

$$H(s) = \frac{\omega_n^2 s}{s^2 + 2\xi\omega_n s + \omega_n^2} \,, \tag{8}$$

where ω_n and ξ respectively denote the natural frequency and damping ratio. Then, the integral terms in (7) can be evaluated[2] as follows:

$$\int_0^{\omega_B} |H(j\omega)|^2 \, d\omega = \frac{\omega_n^3}{4\xi} \left(f_1 + f_2 - f_3\right), \tag{9}$$

where

$$\begin{aligned} f_1 &= \arctan\left(\frac{\omega_B + \omega_n\sqrt{1-\xi^2}}{\xi\omega_n}\right), \\ f_2 &= \arctan\left(\frac{\omega_B - \omega_n\sqrt{1-\xi^2}}{\xi\omega_n}\right), \\ f_3 &= \frac{\xi}{2\sqrt{1-\xi^2}} \ln\left(\frac{\omega_B^2 + 2\omega_B\omega_n\sqrt{1-\xi^2} + \omega_n^2}{\omega_B^2 - 2\omega_B\omega_n\sqrt{1-\xi^2} + \omega_n^2}\right); \end{aligned}$$

and

$$\int_0^{\infty} |H(j\omega)|^2 \, d\omega = \frac{\pi\omega_n^3}{4\xi}. \tag{10}$$

The phase error can be derived in a similar method by evaluating the transfer function between $\phi_{\text{out}}(s)$ and $\phi_{\text{in}}(s)$. For the second-order PLL with lag filter, this transfer function is

$$H'(s) = \frac{\phi_{\text{out}}(s)}{\phi_{\text{in}}(s)} = \frac{K_d K_0 H_{\text{LF}}(s)}{s + K_d K_0 H_{\text{LF}}(s)} = \frac{\omega_n^2}{s^2 + 2\xi\omega_n s + \omega_n^2} \,. \tag{11}$$

The variance $\sigma^2_{\phi_{\text{PLL}}}$ of the phase error can be evaluated in the same way as (7), with

$$\int_0^{\omega_B} |H'(j\omega)|^2 \, d\omega = \frac{\omega_n}{4\xi} \left(f_1 + f_2 + f_3\right), \tag{12}$$

and

$$\int_0^{\infty} |H'(j\omega)|^2 \, d\omega = \frac{\pi\omega_n}{4\xi}. \tag{13}$$

The natural frequency ω_n is related to the necessary training time T_{train}, which is the duration that the PLL spends on adjusting frequencies, also known as the settling time of PLL. For a second-order PLL with lag filter, we have $\omega_n \approx 4/(\xi T_{\text{train}})$ [28]. Because estimation needs to be performed in timeslots 1, 2, and 3, we have $T_{\text{sync}} = 3T_{\text{train}} + T_{\text{ctrl}}$, where T_{ctrl} denotes the duration of control data transmission in timeslot 4.

D. Synchronization Error with MLE

In this subsection, we consider the case where nodes estimate the frequency and phase with the MLE method. Although more sophisticated maximum a posteriori (MAP) based algorithms such as in [29] have been proposed, this part analyzes estimation errors based on the MLE algorithm proposed in [30] which is believed to be more feasible and relaxes the need of huge computational complexity [31], due

[2] We employ Maple [27] to evaluate some sophisticated integrals.

to practical considerations. Different from [30], we consider arbitrary symbol duration (T_s) in our discussion, to better relate the analysis to actual data transmission.

For the received beacon $b_{\text{rcv}}(t)$, when the symbol timing is accurate [32], [33], putting the signal into a pair of orthogonal matched filters and sampling the resulting signal at a time interval of T_s yields a complex signal $\tilde{b}_{\text{rcv}}(kT_s)$ ($k = 1, 2, 3, ...$), where $\left|\tilde{b}_{\text{rcv}}(kT_s)\right|^2$ and $\arg\left(\tilde{b}_{\text{rcv}}(kT_s)\right)$ respectively correspond to the energy and average phase of $b_{\text{rcv}}(t)$ over T_s. Then, likelihood function can be written as

$$\mathcal{L}(\omega_c, \phi) = \left(\frac{1}{\pi N_0}\right)^{N_{\text{train}}} \exp\left(-\sum_{k=0}^{N_{\text{train}}-1} \frac{\left|\tilde{b}_{\text{rcv}}(kT_s) - \sqrt{E_s}\mathrm{e}^{j(\omega_c kT_s+\phi)}\right|^2}{N_0}\right), \tag{14}$$

where N_0 is the variance of AWGN after traversing the matched filter and N_{train} denotes the length of the training sequence. Similarly with [30], by solving

$$\frac{\partial \ln \mathcal{L}(\omega_c, \phi)}{\partial \omega_c} = 0 \quad \text{and} \quad \frac{\partial \ln \mathcal{L}(\omega_c, \phi)}{\partial \phi} = 0\,, \tag{15}$$

we obtain the maximum-likelihood estimators for ω_c and ϕ as

$$\hat{\omega}_{c,\text{MLE}} = \frac{\sum_{k=0}^{N_{\text{train}}-1} kUV \sum_{k=0}^{N_{\text{train}}-1} U - \sum_{k=0}^{N_{\text{train}}-1} UV \sum_{k=0}^{N_{\text{train}}-1} kU}{T_s \sum_{k=0}^{N_{\text{train}}-1} k^2U \sum_{k=0}^{N_{\text{train}}-1} U - T_s\left(\sum_{k=0}^{N_{\text{train}}-1} U\right)^2} \tag{16}$$

and

$$\hat{\phi}_{\text{MLE}} = \frac{\sum_{k=0}^{N_{\text{train}}-1} kUV \sum_{k=0}^{N_{\text{train}}-1} kU - \sum_{k=0}^{N_{\text{train}}-1} k^2U \sum_{k=0}^{N_{\text{train}}-1} UV}{\left(\sum_{k=0}^{N_{\text{train}}-1} kU\right)^2 - \sum_{k=0}^{N_{\text{train}}-1} k^2U \sum_{k=0}^{N_{\text{train}}-1} U}\,, \tag{17}$$

where $U = |b_{\text{rcv}}(kT_s)|$ and $V = \arg\left(b_{\text{rcv}}(kT_s)\right)$.

The variances of estimation errors are bounded by the Cramér-Rao lower bounds by

$$\sigma^2_{\omega_{c,\text{MLE}}} \geq \frac{6N_0}{E_s N_{\text{train}}(N^2_{\text{train}} - 1)T_s^2} \tag{18}$$

and

$$\sigma^2_{\phi_{\text{MLE}}} \geq \frac{N_0(2N_{\text{train}} - 1)}{E_s N_{\text{train}}(N_{\text{train}} + 1)}\,. \tag{19}$$

The lower bounds in (18) and (19) can be attained when the SNR is relatively high, as discussed in [30]. Hence, we use these values as to approximate the variances when using MLE in subsequent discussions.

For MLE, we have $T_{\text{train}} = N_{\text{train}}T_s$ and $T_{\text{trans}} = N_{\text{trans}}T_s$, where N_{trans} denotes the number of transmitted symbols over the transmitting time. Similar to the case of PLL, $T_{\text{sync}} = 3T_{\text{train}} + T_{\text{ctrl}}$, $\Delta\omega_{c,\text{MLE}}$ and $\Delta\phi_{\text{MLE}}$ conform to zero-mean Gaussian distributions respectively given by $\Delta\omega_{c,\text{MLE}} \sim \mathcal{N}(0, \sigma^2_{\omega_{c,\text{MLE}}})$ and $\Delta\phi_{\text{MLE}} \sim \mathcal{N}(0, \sigma^2_{\phi_{\text{MLE}}})$. The impacts of these errors will be analyzed in subsequent sections.

IV. Symbol Error Rate with Estimation Errors

This section analyzes the SER at the relay under the impact of estimation errors studied in the previous section. We first study the SER for M-QAM and quadrature phase shift keying (QPSK) with arbitrary deterministic phase deviations. Then, analytical expression of the average SER over a period of time with random phase deviations is derived. Because a receiver usually performs channel estimation through preambles [34], we assume that the receiver only tracks the phase from knowledge of the preamble at the beginning of each data frame. The receiver is unaware of subsequent phase variations caused by frequency offsets (i.e. $\Delta\omega_c$) in data carrying signals over the transmitting time [35].

A. SER with Deterministic Phase Deviations

To ensure unique decodability for PNC with M-QAM, points in any $\sqrt{M}$ by $\sqrt{M}$ square in the constellation for superposed signals have to be mapped into different symbols [10]. When M is large enough, it is of low probability that the noise can let the superposed signal step over several decision regions and reach a region that should be mapped to a coded symbol that is identical with the correct symbol. Accordingly, we neglect the correct probability of this case in our discussion.

When power control and synchronization are performed, the minimum distance estimation in the 2-dimensional space can be separately performed in the in-phase channel (I-channel) and the quadrature channel (Q-channel). Assume that the transmitted symbols are equiprobable, the error probabilities calculated in both I-channel and Q-channel are equal. For different intervals of decision regions, the error probabilities in the I-channel can be approximated by [24]:

$$P_s\Big|_{m_A,m_B} \approx \begin{cases} Q\left(\frac{d_0 + \mu_0 - \mu}{\sigma_0}\right), & \text{if } m_A, m_B = 1 \\ Q\left(\frac{d_0 + \mu - \mu_0}{\sigma_0}\right), & \text{if } m_A, m_B = \sqrt{M} \\ Q\left(\frac{d_0 + \mu - \mu_0}{\sigma_0}\right) + Q\left(\frac{d_0 + \mu_0 - \mu}{\sigma_0}\right), & \text{else} \end{cases} \tag{20}$$

where $m_A, n_A, m_B, n_B \in \{1, 2, \cdots, \sqrt{M}\}$ respectively represent indices of the M-QAM constellation points in the I-channel and Q-channel from nodes A and B; $\sigma_0 = \sqrt{N_0/2}$ denotes the standard deviation of AWGN in the I-channel; μ_0 denotes the original constellation point without phase deviation in the I-channel and it is given by $\mu_0 = 2(m_A + m_B - 1 - \sqrt{M})d_0$; and μ denotes the constellation point when suffering phase deviation in the I-channel, which is given by $\mu = (2m_A - 1 - \sqrt{M})d_0 \cos\psi_A + (2m_B - 1 - \sqrt{M})d_0 \cos\psi_B - (2n_A - 1 - \sqrt{M})d_0 \sin\psi_A - (2n_B - 1 - \sqrt{M})d_0 \sin\psi_B$. Variables ψ_A and ψ_B represent instantaneous phase deviations (with respect to strict synchronization when the deviations are zero) of S_A and S_B. According to [36], d_0 can be obtained by

$$d_0 = \left(\frac{3E_b \log_2 \sqrt{M}}{M - 1}\right)^{1/2}, \tag{21}$$

where E_b represents the average energy per bit of the received signal at the relay R. For equiprobable symbols, any combination of (m_A, n_A, m_B, n_B) shares the same probability $1/M^2$. Hence the error probability in the I-channel is

$$P_s\Big|_{I\text{-channel}} = \frac{1}{M^2}\sum_{n'_A,n'_B=1}^{\sqrt{M}}\left(P_s\Big|_{m_A,m_B=1} + P_s\Big|_{m_A,m_B=\sqrt{M}} + \sum_{m_A,m_B=1}^{\sqrt{M}} P_s\Big|_{m_A+m_B\neq 2,2\sqrt{M}}\right). \quad (22)$$

Then, the SER for M-QAM modulated PNC with deterministic phase deviations can be evaluated by

$$P_s = 1 - \left(1 - P_s\Big|_{I-\text{channel}}\right)^2. \quad (23)$$

When using QPSK, the approximated results (which neglect constellation points that are mapped to identical symbols) can become inaccurate, because there is only one other decision region between those regions that are to be mapped to the same symbol. Therefore, we evaluate the exact SER for QPSK. The in-phase component of the superposed constellation is given by $I_R(m_\Sigma) \in \{-2d_0, 0, 2d_0\}$, and the mapping rule is that $\{-2d_0, 2d_0\}$ is mapped to bit "0" (or, correspondingly, "1") and $\{0\}$ is mapped to bit "1" (or, correspondingly, "0"). Thus, cases of $m_A, m_B = 1$ and $m_A, m_B = \sqrt{M}$ in (20) can be combined as

$$P'_s\Big|_{m_A,m_B=1 \text{ or } \sqrt{M}} = Q\left(\frac{\mu - d_0}{\sigma_0}\right) - Q\left(\frac{\mu + d_0}{\sigma_0}\right). \quad (24)$$

Let (24) be the substitutes for cases of $m_A, m_B = 1$ and $m_A, m_B = \sqrt{M}$ in (20), the exact SER for QPSK modulated PNC with phase deviation can be calculated with (23).

B. Average SER with Random Phase over A Segment of Time

The phase deviation accumulates with time due to the presence of frequency estimation error. Because the transmitting time is usually much longer than the duration of the training sequence, the phase deviation can accumulate to a value which is much larger than the initial phase estimation error. Therefore, we mainly focus on phase deviation caused by frequency error in this subsection.

Remark that in the following analysis, we only focus on ψ_A due to the similarity between ψ_A and ψ_B. As depicted in Fig. 4, the instantaneous phase deviation $\psi_A(t)$ is given by $\psi_A(t) = t\psi_{A,\text{max}}/T_{\text{trans}}$, where $\psi_{A,\text{max}}$ denotes the maximum phase deviation at the end of each data transmission. The phase deviation process is a cyclostationary process with $T_{\text{sync}} + T_{\text{trans}}$ as the period. Due to the relationship given by $\psi_{A,\text{max}} = \Delta\omega_c T_{\text{trans}}$, both $\psi_{A,\text{max}}$ and $\psi_A(t)$ follow zero-mean Gaussian distributions. The variance of $\psi_{A,\text{max}}$ is denoted by $\sigma^2_{A,\text{max}}$, and $\sigma^2_{A,\text{max}} = T^2_{\text{trans}}\sigma^2_{\omega_c}$. It follows that the instantaneous variance of $\psi_A(t)$ is

$$\sigma^2_A(t) = \frac{t^2}{T^2_{\text{trans}}}\sigma^2_{A,\text{max}}. \quad (25)$$

Then, the expectation of the SER at time instant t is

$$\overline{P_s}(t) = \int_{-\infty}^{+\infty}\int_{-\infty}^{+\infty} P_s(\psi_A,\psi_B)p(\psi_A,\psi_B,t)\,d\psi_A d\psi_B\,, \quad (26)$$

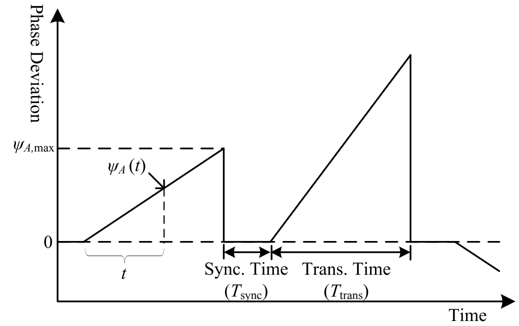

Fig. 4. Phase deviation at end node A. Phase deviation increases linearly due to the frequency estimation error that is generated during synchronization. Random frequency errors cause different deviations in different transmission phases. Similar phenomenon can be observed at end node B.

where P_s is calculated with (23) under different values of ψ_A and ψ_B, $p(\psi_A, \psi_B, t)$ stands for the joint probability density function of $\psi_A(t)$ and $\psi_B(t)$. Because $\psi_A(t)$ and $\psi_B(t)$ are independently distributed, and $\psi_A(t) \sim \mathcal{N}(0, \sigma^2_A(t))$, $\psi_B(t) \sim \mathcal{N}(0, \sigma^2_B(t))$, we have

$$p(\psi_A,\psi_B,t) = \frac{1}{2\pi\sigma_A(t)\sigma_B(t)}\mathrm{e}^{-\frac{\psi_A^2}{2\sigma_A^2(t)} - \frac{\psi_B^2}{2\sigma_B^2(t)}} \quad (27)$$

The average SER for over the whole transmitting time during the MA phase is then given by

$$\overline{P_{s,\text{MA}}} = \frac{1}{T_{\text{trans}}}\int_0^{T_{\text{trans}}} \overline{P_s}(t)\,dt. \quad (28)$$

C. Approximate Analytical Solution

Due to the absence of explicit expressions for (26) and (28) and the complexity when calculating numerical integrations, in this subsection, we derive an approximate solution to (26) and (28).

Assume that the instantaneous phase deviations are small, i.e. $\psi(t) \approx 0$, we have $\sin(\psi(t)) \approx \psi(t)$ and $\cos(\psi(t)) \approx 1$. Substituting these approximations into (20), and recalling that $\psi_A(t)$ and $\psi_B(t)$ are Gaussian random variables, $\Delta\mu(t) = \mu(t) - \mu_0(t)$ can be regarded as a Gaussian random variable with zero mean and variance $\sigma^2_\mu(n_A, n_B, t) = (2n_A - 1 - \sqrt{M})^2 d_0^2\sigma_A^2(t) + (2n_B - 1 - \sqrt{M})^2 d_0^2\sigma_B^2(t)$. Further, by ignoring the square terms in (23), we achieve $P_s \approx 2P_s\big|_{I-\text{channel}}$, and the integral[3] in (26) can be performed on each term corresponding to one Q-Function in (20). Considering that

$$Q(x) \approx Q_{\text{approx}}(x) \triangleq \begin{cases} \frac{1}{2}\mathrm{e}^{-\frac{x^2}{2}} & \text{if } x \geq 0 \\ 1 - \frac{1}{2}\mathrm{e}^{-\frac{x^2}{2}} & \text{if } x < 0 \end{cases}, \quad (29)$$

[3] Note that the integral can be written as a one dimensional integral now, because we consider a single Gaussian variable $\Delta\mu$ here.

the integrated value for each term in (20) is[4]

$$F(t) = \frac{1}{\sqrt{2\pi}\sigma_\mu(t)} \int_{-\infty}^{+\infty} Q_{\text{approx}} \left(\frac{d_0 \pm \Delta\mu}{\sigma_0} \right) \mathrm{e}^{-\frac{(\Delta\mu)^2}{2\sigma_\mu^2(t)}} \, d(\Delta\mu)$$
$$= \frac{\sigma_0 \operatorname{erf}\left(\frac{d_0 \sigma_0}{\sigma_\mu(t)\sqrt{2\sigma_0^2 + 2\sigma_\mu^2(t)}} \right) \mathrm{e}^{-\frac{d_0^2}{2\sigma_0^2 + 2\sigma_\mu^2(t)}}}{2\sqrt{\sigma_0^2 + \sigma_\mu^2(t)}} + Q\left(\frac{d_0}{\sigma_\mu(t)} \right). \tag{30}$$

Summing up the result in (30) for all the indices $m_A, n_A, m_B, n_B \in \{1, 2, ..., \sqrt{M}\}$ as in (22) and multiplying by two yields the approximate result for (26).

To obtain an approximate result for (28), we perform an asymptotic analysis. When $\sigma_0 \to 0$, the first term in (30) vanishes to zero. Again, using $Q(x) \approx \frac{1}{2}\mathrm{e}^{-\frac{x^2}{2}}$ for $x \geq 0$ and $\sigma_\mu(t) = t\sigma_{\mu,\max}/T_{\text{trans}}$, where $\sigma_{\mu,\max}$ denotes the standard deviation of $\Delta\mu$ at the end of each data transmission, we have

$$F(t)\Big|_{\sigma_0 \to 0} \approx \frac{1}{2}\mathrm{e}^{-\frac{d_0^2 T_{\text{trans}}^2}{2t^2\sigma_{\mu,\max}^2}}. \tag{31}$$

Taking its logarithm yields

$$\ln\left(2F(t)\right)\Big|_{\sigma_0 \to 0} \approx -\frac{d_0^2 T_{\text{trans}}^2}{2t^2\sigma_{\mu,\max}^2}. \tag{32}$$

It follows that

$$\frac{\ln\left(2F(t)\right)}{\ln\left(2F(T_{\text{trans}})\right)}\Bigg|_{\sigma_0 \to 0} \approx \frac{T_{\text{trans}}^2}{t^2}, \tag{33}$$

and

$$F(t)|_{\sigma_0 \to 0} \approx \frac{\left(2F(T_{\text{trans}})\right)^{\frac{T_{\text{trans}}^2}{t^2}}}{2}\Bigg|_{\sigma_0 \to 0}. \tag{34}$$

Relaxing the constraint of $\sigma_0 \to 0$, the average value of one term in (20) can be approximated by

$$\overline{F} \approx \frac{1}{2T_{\text{trans}}} \int_0^{T_{\text{trans}}} \left(2F(T_{\text{trans}})\right)^{\frac{T_{\text{trans}}^2}{t^2}} dt$$
$$= F(T_{\text{trans}}) - \sqrt{-\pi \cdot F_{\ln}}\, Q\left(\sqrt{-2F_{\ln}}\right), \tag{35}$$

where $F_{\ln} = \ln(2F(T_{\text{trans}}))$. The approximate result for (28) can then be evaluated by summing up the result in (35) for all the indices $m_A, n_A, m_B, n_B \in \{1, 2, ..., \sqrt{M}\}$ as in (22) and multiplying by two.

D. Numerical Results

We perform Monte Carlo simulations to verify the analytical results. Figs. 5 and 6 show the comparison among simulation results, analytical results evaluated by (28) using numerical integration, and approximate analytical results derived in Section IV-C. We consider the case where $\sigma_{A,\max}^2 = \sigma_{B,\max}^2 = \sigma_{\max}^2$.

The results indicate agreements between analytical results, approximate analytical results, and simulation results. It can be observed that with both 16-QAM and QPSK, the average SER curves do not always fall as SNR increases, but level off and converge to stable values at some values of $\sigma_{\max}$. The reason is

[4]For simplicity, we omit the variables n_A and n_B.

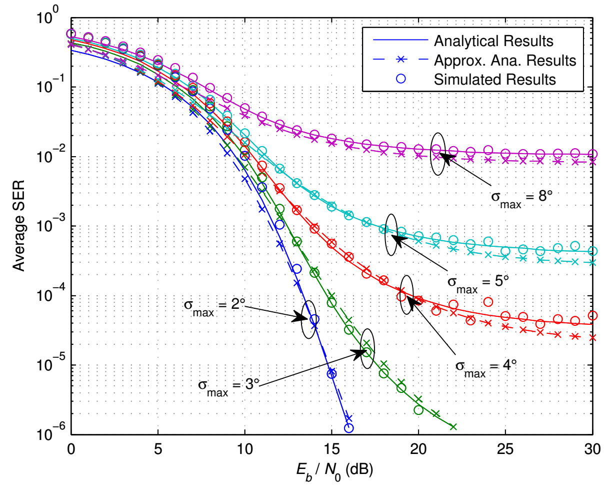

Fig. 5. Average SER for 16-QAM modulated PNC.

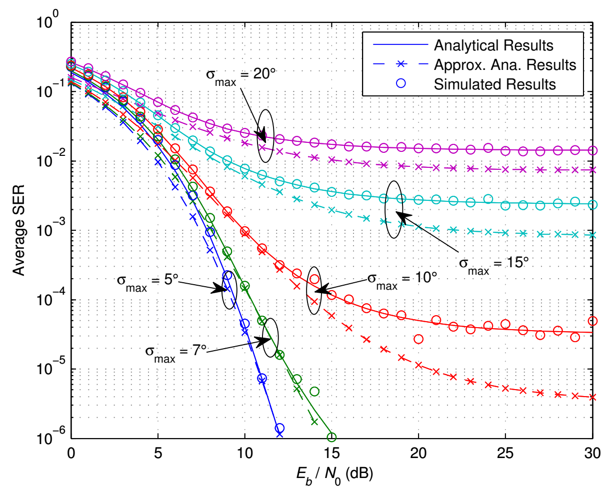

Fig. 6. Average SER for QPSK modulated PNC.

that in high SNR regions, the symbol error is mainly caused by phase deviations, therefore the SER does not decrease much with increasing SNR as long as the value of $\sigma_{\max}$ remains unchanged. The approximate analytical results are not very accurate when $\sigma_{\max}$ is large, as shown in Fig. 6, because the assumption $\sin\psi \approx \psi$ only holds for small phase deviations.

V. Goodput Performance Analysis

This section investigates the goodput (i.e. the amount of successfully transmitted information) performance for PNC under the joint impact from synchronization overhead and increased SER caused by phase deviations.

A. Analytical Evaluation

Recall that in a two-way relay network with bidirectional flows, the ideal throughput for conventional network coding (CNC) and PNC are respectively $2/3\log_2 M$ and $\log_2 M$ [2]. Considering synchronization overhead and packet loss, the goodput for PNC is

$$G_{\text{PNC}} = \frac{1}{2}(1-\rho)(1-\overline{P_{s,\text{MA}}})^{N_{\text{pk}}}(1-P_{s,\text{BC},A})^{N_{\text{pk}}}\log_2 M + \frac{1}{2}(1-\rho)(1-\overline{P_{s,\text{MA}}})^{N_{\text{pk}}}(1-P_{s,\text{BC},B})^{N_{\text{pk}}}\log_2 M, \quad (36)$$

where ρ denotes the synchronization overhead in percentages. When the transmission rate remains unchanged, the transmitting time in the MA phase equals that in the BC phase. Then, we have

$$\rho = T_{\text{sync}}/(T_{\text{sync}} + 2T_{\text{trans}}). \quad (37)$$

The value of $(1-\overline{P_{s,\text{MA}}})^{N_{\text{pk}}}$ is the packet success rate at R over the MA phase, where N_{pk} denotes the packet length and $\overline{P_{s,\text{MA}}}$ is the average SER during MA phase which can be evaluated by (28). Likewise, $(1-P_{s,\text{BC},A})^{N_{\text{pk}}}$ and $(1-P_{s,\text{BC},B})^{N_{\text{pk}}}$ are respectively the packet success rates at nodes A and B in the BC phase, where $P_{s,\text{BC},A}$ and $P_{s,\text{BC},B}$ respectively represent SERs for common M-QAM at nodes A and B. The SER for M-QAM is given by [37]:

$$P_{M-\text{QAM}} = 4\left(\frac{\sqrt{M}-1}{\sqrt{M}}\right)Q\left(\sqrt{\frac{3E_s}{N_0(M-1)}}\right) - 4\left(\frac{\sqrt{M}-1}{\sqrt{M}}\right)^2 Q^2\left(\sqrt{\frac{3E_s}{N_0(M-1)}}\right). \quad (38)$$

Likewise, the goodput for CNC is

$$G_{\text{CNC}} = \frac{1}{2}\cdot\frac{2\log_2 M}{3}(1-P_{s,B,R})^{N_{\text{pk}}}(1-P_{s,R,A})^{N_{\text{pk}}} + \frac{1}{2}\cdot\frac{2\log_2 M}{3}(1-P_{s,A,R})^{N_{\text{pk}}}(1-P_{s,R,B})^{N_{\text{pk}}}, \quad (39)$$

where $P_{s,B,R}$, $P_{s,A,R}$, $P_{s,R,A}$, and $P_{s,R,B}$ respectively denote the SERs for corresponding uplinks ($B \to R$ and $A \to R$) and downlinks ($R \to A$ and $R \to B$), and these probabilities can also be evaluated by (38).

B. Impact of Training Sequence Time-Length

The training sequence time-length T_{train} has a trade-off effect on the goodput when using PNC. Recall that $T_{\text{sync}} = 3T_{\text{train}} + T_{\text{ctrl}}$ as discussed in Section III-B, a larger value of T_{train} yields longer synchronization time, which may increase the overhead. However, a larger T_{train} also results in a more precise phase and frequency estimation, which could increase the packet success rate and, subsequently, the goodput.

Therefore, an appropriate value of T_{train} should be selected to maximize the goodput. This can be formulated as the following optimization problem:

$$\max_{T_{\text{train}}} \; G_{\text{PNC}} \quad s.t. \;\; 0 \le T_{\text{train}} \le \frac{1}{3}(T_c - T_{\text{ctrl}}), \quad (40)$$

where T_c denotes the period of the synchronization cycle. We solve (40) using numerical evaluation methods in MATLAB. Fig. 7 shows the optimal T_{train} under different values of E_b/N_0 (i.e. SNR per bit), where E_b denotes the energy per bit, when using the MLE method and the approximate solution as discussed in Section IV-C for evaluation.

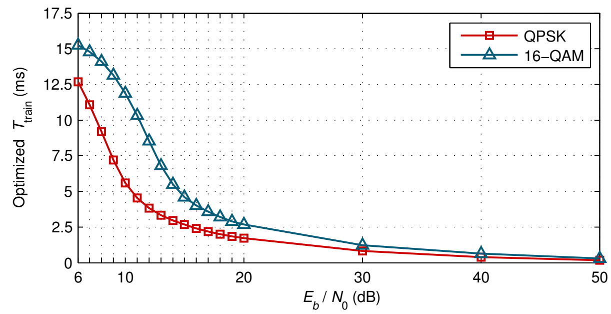

Fig. 7. Optimized T_{train} values under different SNRs when using the MLE method.

C. Numerical Results

The goodput performance of synchronous PNC is evaluated numerically in this subsection. We consider PNC with both PLL and MLE based synchronization methods (notated as PLL-PNC and MLE-PNC in the following discussions), and also compare with the goodput of CNC.

In our simulations, we set $T_c = 64$ ms, which corresponds to the channel coherence time (i.e. the time that the channel almost remains unchanged) of fixed nodes with 2.4 GHz radio transceivers in fast varying environments [35]. The transmitting time T_{trans} is then $T_{\text{trans}} = T_c - T_{\text{sync}}$. The symbol duration T_s is set to $1\,\mu$s, and the packet length N_{pk} is set to 1024 bytes. The duration of control data T_{ctrl} is set to 0.3 ms, which is enough for transmitting several hundred bits. For the PLL, the values of ξ and N_p are respectively set to 0.707 and $7.0 \times 10^{-11}\,\text{Hz}^{-1}$ [17], [26].

Regarding the value of T_{train}, we consider both fixed and optimal value settings. For the fixed value setting, we set $T_{\text{train}} = 5$ ms and evaluate the performance of PLL-PNC and MLE-PNC, respectively. We select $T_{\text{train}} = 5$ ms because it is close to the optimal T_{train} corresponding to the minimum E_b/N_0 requirement for QPSK and 16-QAM, as shown in Fig. 7. For the optimal value setting, we set T_{train} to the optimal values as in Fig. 7 and only evaluate the performance of MLE-PNC. We do not evaluate the performance of PLL-PNC with optimal T_{train}, because the settling time of the PLL is a designed hardware parameter which is difficult to adjust based on E_b/N_0. However, when using the MLE based estimation method, it is possible to adapt the training sequence length to E_b/N_0.

The goodputs when using different techniques are shown in Fig. 8. It can be observed that, when $T_{\text{train}} = 5$ ms, the goodputs of MLE-PNC and PLL-PNC both converge to stable values that correspond to a goodput gain of approximately 1.30 over CNC, for both 16-QAM and QPSK modulations. Such a convergence is because, at high SNR values, the packet loss is very low so that the goodput does not vary much with the SNR. The difference between the observed goodput gain and the maximal throughput gain (which is 1.5) is due to the overhead. With our simulation settings, according to (37), the overhead $\rho = 15.3/(15.3+2\times 48.7) = 0.136$. The goodput gain with the given overhead can be evaluated by $1.5(1-\rho) = 1.30$, which matches with the numerical results. At medium SNR values,

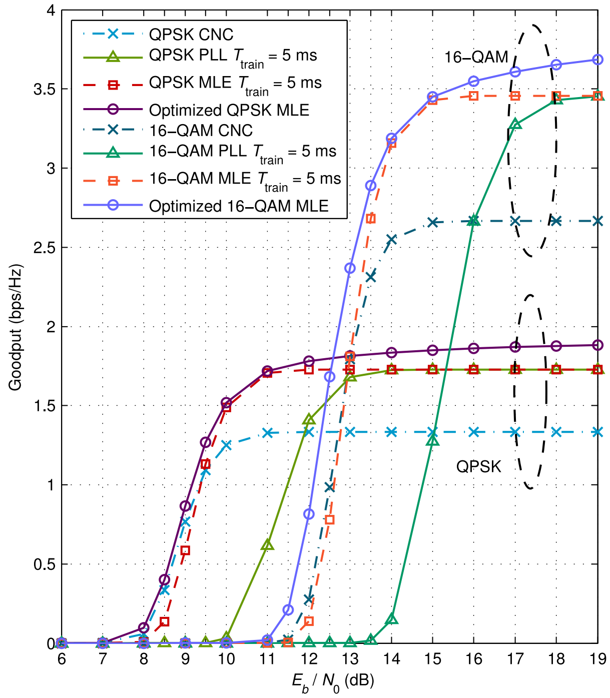

Fig. 8. Comparison between the goodput of synchronous PNC and that of CNC.

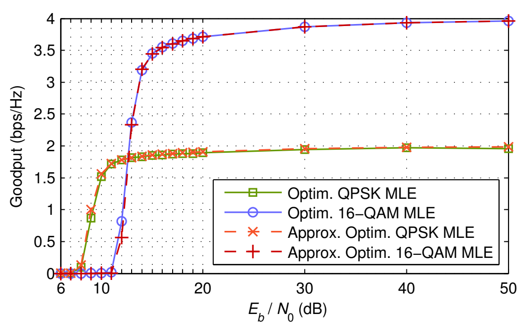

Fig. 9. Actual and approximated goodput of MLE-PNC with optimized T_{train}.

we can see that MLE-PNC outperforms PLL-PNC, because MLE provides higher estimation accuracy and the goodput is affected by the packet loss in this SNR region.

For both 16-QAM and QPSK, MLE-PNC with optimized T_{train} outperforms the other schemes, and its goodput keeps increasing with E_b/N_0. This is because the value of T_{train} is optimized based on the SNR. At high SNRs, T_{train} can be considerably small, yielding a very small overhead. The goodput at some higher SNR values is plotted in Fig. 9. We can observe that, when $E_b/N_0 = 50$ dB, the goodput gain is approximately 1.48, which is very close to the maximal throughput gain. Also, the goodputs evaluated with the analytical approximate solutions as discussed in IV-C matches with their actual values.

VI. Conclusions

In this paper, we have analyzed the feasibility of PNC with phase-level synchronization. We have proposed a synchronization scheme for PNC. Subsequently, we have revealed analytical relationships among the goodput, average SER, synchronization overhead, and estimation errors, when using either PLL or MLE based synchronization techniques. Numerical results show that the goodput of a two-way relay network can benefit from synchronous PNC, and MLE based synchronization schemes can attain more goodput gain than PLL based schemes. Our study also reveals that higher goodput can be obtained by adjusting the training sequence length according to the SNR. The goodput evaluated in this paper is based on symbols without channel coding. We would foresee that the goodput performance of synchronous PNC could be further improved when channel coding is performed. Although the error analysis in this paper focuses on phase and frequency estimation errors, it can be easily generalized to incoporate some other error terms, using the same analytical framework. The results in this paper provide some insights and benchmarks for the implementation of synchronous PNC. In the future, we will focus on the impact of estimation errors on asynchronous PNC schemes, because asynchronous PNC also requires phase and frequency tracking (although adjustment is not needed), which introduces estimation errors similarly as synchronous PNC.

References

[1] Y. Huang, Q. Song, S. Wang, and A. Jamalipour, "Phase-level synchronization for physical-layer network coding," in *Proc. IEEE GLOBECOM 2012*, Dec. 2012, pp. 4423–4428.

[2] S. Zhang, S. C. Liew, and P. P. Lam, "Hot topic: Physical-layer network coding," in *Proc. ACM MobiCom 2006*, Sep. 2006, pp. 358–365.

[3] P. Popovski and H. Yomo, "The anti-packets can increase the achievable throughput of a wireless multi-hop network," in *Proc. IEEE ICC 2006*, Jun. 2006, pp. 3885–3890.

[4] K. Lee and L. Hanzo, "Resource-efficient wireless relaying protocols," *IEEE Wireless Commun. Mag.*, vol. 17, no. 2, pp. 66–72, Apr. 2010.

[5] T. Koike-Akino, P. Popovski, and V. Tarokh, "Optimized constellations for two-way wireless relaying with physical network coding," *IEEE J. Sel. Areas Commun.*, vol. 27, no. 5, pp. 773–787, Jun. 2009.

[6] L. Lu, S. C. Liew, and S. Zhang, "Optimal decoding algorithm for asynchronous physical-layer network coding," in *Proc. IEEE ICC 2011*, Jun. 2011, pp. 1–6.

[7] T. Yang and I. Collings, "Asymptotically optimal error-rate performance of linear physical-layer network coding in rayleigh fading two-way relay channels," *IEEE Commun. Lett.*, vol. 16, no. 7, pp. 1068 –1071, Jul. 2012.

[8] M. Noori and M. Ardakani, "On symbol mapping for binary physical-layer network coding with PSK modulation," *IEEE Trans. Wireless Commun.*, vol. 11, no. 1, pp. 21–26, Jan. 2012.

[9] H. J. Yang, Y. Choi, and J. Chun, "Modified high-order PAMs for binary coded physical-layer network coding," *IEEE Commun. Lett.*, vol. 14, no. 8, pp. 689 –691, Aug. 2010.

[10] S. Wang, Q. Song, L. Guo, and A. Jamalipour, "Constellation mapping for physical-layer network coding with M-QAM modulation," in *Proc. IEEE GLOBECOM 2012*, Dec. 2012, pp. 4429–4434.

[11] M. P. Wilson, K. Narayanan, H. D. Pfister, and A. Sprintson, "Joint physical layer coding and network coding for bidirectional relaying," *IEEE Trans. Inf. Theory*, vol. 56, no. 11, pp. 5641–5654, Nov. 2010.

[12] W. Nam, S.-Y. Chung, and Y. H. Lee, "Capacity of the gaussian two-way relay channel to within 1/2 bit," *IEEE Trans. Inf. Theory*, vol. 56, no. 11, pp. 5488–5494, Nov. 2010.

[13] K. Yasami, A. Razi, and A. Abedi, "Analysis of channel estimation error in physical layer network coding," *IEEE Commun. Lett.*, vol. 15, no. 10, pp. 1029–1031, Oct. 2011.

[14] T. Koike-Akino, P. Popovski, and V. Tarokh, "Adaptive modulation and network coding with optimized precoding in two-way relaying," in *Proc. IEEE GLOBECOM 2009*, Nov. 2009, pp. 1–6.

[15] S. Zhang, S.-C. Liew, and P. P. Lam, "On the synchronization of physical-layer network coding," in *Proc. IEEE Information Theory Workshop 2006*, Oct. 2006, pp. 404–408.

[16] S. Sigg, R. M. E. Masri, and M. Beigl, “Feedback-based closed-loop carrier synchronization: A sharp asymptotic bound, an asymptotically optimal approach, simulations, and experiments,” *IEEE Trans. Mobile Comput.*, vol. 10, no. 11, pp. 1605–1617, Nov. 2011.
[17] R. Mudumbai, G. Barriac, and U. Madhow, “On the feasibility of distributed beamforming in wireless networks,” *IEEE Trans. Wireless Commun.*, vol. 6, no. 5, pp. 1754–1763, May 2007.
[18] D. R. Brown and H. V. Poor, “Time-slotted round-trip carrier synchronization for distributed beamforming,” *IEEE Trans. Signal Process.*, vol. 56, no. 11, pp. 5630–5643, Nov. 2008.
[19] D. R. Brown, B. Zhang, B. Svirchuk, and M. Ni, “An experimental study of acoustic distributed beamforming using round-trip carrier synchronization,” in *Proc. IEEE ARRAY 2010*, Oct. 2010, pp. 316–323.
[20] S. Wang, Q. Song, X. Wang, and A. Jamalipour, “Rate and power adaptation for analog network coding,” *IEEE Trans. Veh. Technol.*, vol. 60, no. 5, pp. 2302–2313, Jun. 2011.
[21] K. Lu, S. Fu, Y. Qian, and H.-W. Chen, “SER performance analysis for physical layer network coding over AWGN channels,” in *Proc. IEEE GLOBECOM 2009*, Dec. 2009, pp. 1–6.
[22] M. Park, I. Choi, and I. Lee, “Exact BER analysis of physical layer network coding for two-way relay channels,” in *Proc. IEEE VTC 2011*, May 2011, pp. 1–5.
[23] M. Ju and I.-M. Kim, “Error performance analysis of BPSK modulation in physical-layer network-coded bidirectional relay networks,” *IEEE Trans. Commun.*, vol. 58, no. 10, pp. 2770–2775, Oct. 2010.
[24] Y. Huang, Q. Song, S. Wang, and A. Jamalipour, “Symbol error rate analysis for M-QAM modulated physical-layer network coding with phase errors,” in *Proc. IEEE PIMRC 2012*, Sep. 2012, pp. 2003–2008.
[25] S. Wang, Q. Song, X. Wang, and A. Jamalipour, “Distributed MAC protocol supporting physical-layer network coding,” *IEEE Trans. Mobile Comput.*, vol. 12, no. 5, pp. 1023–1036, May 2013.
[26] F. M. Gardner, *Phaselock Techniques*, 3rd ed. Hoboken: John Wiley & Sons, 2005.
[27] Maple 15. [Online]. Available: http://www.maplesoft.com
[28] F. Golnaraghi and B. C. Kuo, *Automatic Control System*. New York: John Wiley & Sons, 2003.
[29] H. Fu and P. Y. Kam, “Weighted phase averager for frequency estimation of a noisy single sinusoid: Application of the observation phase noise model,” in *Proc. IEEE PIMRC 2009*, Sep. 2009, pp. 1923–1927.
[30] ——, “MAP/ML estimation of the frequency and phase of a single sinusoid in noise,” *IEEE Trans. Signal Process.*, vol. 55, no. 3, pp. 834–845, Mar. 2007.
[31] D. Rife and R. Boorstyn, “Single tone parameter estimation from discrete-time observations,” *IEEE Trans. Inf. Theory*, vol. 20, no. 5, pp. 591–598, Sep. 1974.
[32] G. Tavares, L. Tavares, and A. Petrolino, “On the true cramer-rao lower bound for data-aided carrier-phase-independent frequency offset and symbol timing estimation,” *IEEE Trans. Commun.*, vol. 58, no. 2, pp. 442–447, Feb. 2010.
[33] S. Chang and B. Kelley, “An efficient time synchronization scheme for broadband two-way relaying networks based on physical-layer network coding,” *IEEE Commun. Lett.*, vol. 16, no. 9, pp. 1416 –1419, Sep. 2012.
[34] W. U. Bajwa, J. Haupt, A. M. Sayeed, and R. Nowak, “Compressed channel sensing: A new approach to estimating sparse multipath channels,” *Proc. IEEE*, vol. 98, no. 6, pp. 1058–1076, Jun. 2010.
[35] E. Aryafar, M. Khojastepour, K. Sundaresan, S. Rangarajan, and E. W. Knightly, “ADAM: An adaptive beamforming system for multicasting in wireless LANs,” in *Proc. IEEE INFOCOM 2012*, Mar. 2012, pp. 1467–1475.
[36] J. G. Proakis, *Digital Communications*, 4th ed. Boston: McGraw-Hill, 2001.
[37] M. K. Simon and M.-S. Alouini, *Digital Communication over Fading Channels*, 2nd ed. New York: Wiley, 2005.

Yang Huang received the Bachelor’s degree from Northeastern University, China, in 2011. Currently, he is pursuing the Master’s degree in Electronics and Communication Engineering, at Northeastern University, China. His general research interests lie in communication systems, cooperative communications, network coding, and radio resource management. He is a student member of the IEEE.

Shiqiang Wang received the BEng and MEng degrees from Northeastern University, China, in 2009 and 2011, respectively. He is currently working toward the PhD degree in the Department of Electrical and Electronic Engineering, Imperial College London, United Kingdom. His research interests include network coding, protocol design, optimization, and prototyping for wireless networks. He has a dozen scholarly publications in international journals and conferences. He served on the program committee of IEEE VTC 2012-Fall, 2013-Spring, and 2013-Fall.

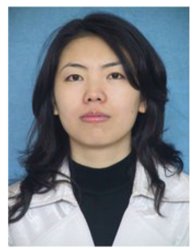

Qingyang Song received the PhD degree in telecommunications engineering from the University of Sydney, Australia. She is an associate professor at Northeastern University, China. She has authored more than 30 papers in major journals and international conferences. These papers have been cited more than 500 times in scientific literature. Her current research interests are in radio resource management, network coding, cognitive radio networks, and cooperative communications. She is a member of the IEEE.

Lei Guo received the Ph.D. degree in communication and information systems from School of Communication and Information Engineering, University of Electronic Science and Technology of China, Chengdu, China, in 2006. He is currently a professor in College of Information Science and Engineering, Northeastern University, Shenyang, China. His research interests include optical networks, access networks, network optimization and wireless communications. He has published over 200 technical papers in the above areas on international journals and conferences, such as IEEE Trans. Commun., IEEE/OSA J. Lightwave Technol., IEEE Commun. Lett., IEEE GLOBECOM, IEEE ICC, etc. Dr. Guo is a member of IEEE and OSA, and is also a senior member of China Institute of Communications. He is now serving as an editor for three international journals.

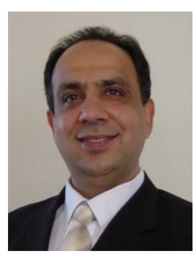

Abbas Jamalipour (S’86-M’91-SM’00-F’07) received the Ph.D. degree from Nagoya University, Nagoya, Japan. He is the Chair Professor of Ubiquitous Mobile Networking with the School of Electrical and Information Engineering, University of Sydney, Sydney, NSW, Australia. He is a Fellow of the Institute of Electrical, Information, and Communication Engineers (IEICE) and the Institution of Engineers Australia, an IEEE Distinguished Lecturer, and a Technical Editor of several scholarly journals. He has been a Chair of several international conferences, including the IEEE International Conference on Communications and the IEEE Global Communications Conference, General Chair of the 2010 IEEE Wireless Communications and Networking Conference, as well as being the technical program chair of IEEE PIMRC2012 and IEEE ICC2014. He is the Vice President - Conferences and a member of Board of Governors of the IEEE Communications Society (ComSoc). He is the recipient of several prestigious awards, including the 2010 IEEE ComSoc Harold Sobol Award for Exemplary Service to Meetings and Conferences, the 2006 IEEE ComSoc Distinguished Contribution to Satellite Communications Award, and the 2006 IEEE ComSoc Best Tutorial Paper Award.